Hippocampal Pyramidal Neuron Size Differs Among Subfields: Implications for Subfield Parcellation

Emily M. Williams
Massachusetts General Hospital
Josue Llamas-Rodriguez
Massachusetts General Hospital
Samantha Champion
Massachusetts General Hospital
Melanie Lang-Orsini
Massachusetts General Hospital
Matthew P. Frosch
Massachusetts General Hospital
Jean C. Augustinack (jaugustinack@mgh.harvard.edu)
Massachusetts General Hospital

Research Article

Keywords: Hippocampus, Parcellation, Feret's diameter, Neuronal width, Histology

Posted Date: May 16th, 2022

DOI: https://doi.org/10.21203/rs.3.rs-1646790/v1

Abstract

The hippocampus is integral for learning and memory and is targeted by multiple diseases and disorders such as anxiety, depression, epilepsy, and Alzheimer's disease. Neuroimaging approaches frequently use hippocampal or subfield volumes as a standard measure of neurodegeneration, thus making it an essential biomarker to study. However, *in vivo* MRI lacks the resolution needed to accurately parcellate subfields, and histologic delineations rely on vague or outdated features. More so, several discrepancies exist in subfield segmentation among groups. The present study sought to advance the histology segmentation field by acquiring quantitative neuron width measurements of the hippocampal subfields from 18 postmortem human samples. Neuron widths were collected using Feret's diameter on hippocampal pyramidal neurons at five distinct anterior-posterior levels. Measurements were collected from CA1, CA2, CA3, CA4 and subiculum and the uncinate (medial) counterparts (CA1u, CA2u, CA3u, Subu). Ten neurons were measured per subfield per level, resulting in a total of 5,430 measured neurons. Our measurements indicate the following order of neuron size: CA4 > CA3 = CA2 > CA1 = Sub > ParaSub > PreSub. We also observed that each medial (uncinate) subfield had smaller neurons than its lateral counterpart (e.g., CA1 > CA1u). Further, we found that right hemisphere hippocampi had significantly larger neurons than left hemisphere hippocampi, and that controls had larger neurons than early Braak & Braak staged cases. The findings provide quantitative ground truth histologic measures for pyramidal neurons within individual subfields and a reliable method to distinguish the subfields at differing anterior-posterior levels.

Introduction

It is well established that the hippocampus is crucial for learning and memory (Buzsáki and Moser, 2013; Hannula et al., 2006; O'Keefe et al., 1998; Rubin et al., 2014; Squire, 2004; Warren et al., 2012). The hippocampal formation is a complex structure, which includes the cornu ammonis subfields (CA1-4), dentate gyrus (DG), and subicular cortices (subiculum [Sub], presubiculum [PreSub or PrS], and parasubiculum [ParaSub or PaS]) (Ding and Van Hoesen, 2015; Duvernoy, 2005; Rosene and Van Hoesen, 1987). Numerous diseases target the hippocampus, such as Alzheimer's disease (Braak et al., 2006; Braak and Braak, 1991; Jaroudi et al., 2017), epilepsy (Dam, 1980; de Lanerolle et al., 1989; Engel, 1996), schizophrenia (Harrison, 2004; Heckers et al., 1998; Zhou et al., 2008), and post-traumatic stress disorder (PTSD) (Bonne et al., 2008; Harnett et al., 2020; Logue et al., 2018).

Hippocampal volume is used as a standard measure of neurodegeneration in neuroimaging, especially structural MRI, thus making it a frequently used biomarker (Bosco et al., 2017). Substantial progress has been made in segmenting the hippocampus as a whole structure as well as harmonizing that effort (Boccardi et al., 2015; Bosco et al., 2017; Frisoni and Jack, 2011). Segmentation of the hippocampal subfields has also progressed due to multiple groups producing hippocampal subfield atlases (Adler et al., 2018, 2014; de Flores et al., 2020; Iglesias et al., 2015; Parekh et al., 2015) and to a large collaborative effort from the hippocampal subfields segmentation group to harmonize these efforts (Olsen et al., 2019; Wisse et al., 2017; Yushkevich et al., 2015). Although neuroimaging studies have reported both

functionalities and vulnerabilities of the hippocampal subfields (de Flores et al., 2015; Goubran et al., 2015; Mueller et al., 2007; Pan et al., 2021; Raz et al., 2015; Tardif et al., 2017; Zeidman et al., 2015), a cohesive thread has yet to emerge. This could be attributed to the fact that the neuroimaging field is outpacing the neuroanatomy field, as neuroanatomy studies do not always agree on subfield boundaries (de Flores et al., 2020; Ding, 2013; Ding and Van Hoesen, 2015; Insausti et al., 2017; Olsen et al., 2019; Palomero-Gallagher et al., 2020). The reason for the discrepancies is that identifying criteria for subfields lack clarity and distinctiveness, which leads to individual interpretation. Such disagreements, combined with the low resolution in *in vivo* MRI, have led some neuroimagers to base their segmentations on angles or extrapolations (Bender et al., 2017; Mueller et al., 2007; Raz et al., 2015; Steve et al., 2017) rather than the cytoarchitecture of the subfields.

There has been progress in recent years in cytoarchitectonic-grounded parcellations (Adler et al., 2014; de Flores et al., 2020; Ding, 2013; Ding and Van Hoesen, 2015; Insausti et al., 2017; Palomero-Gallagher et al., 2020; Rosene and Van Hoesen, 1987), yet discrepances among many of the subfield parcellations persist. For instance, some authors combine CA3 and CA4 (de Flores et al., 2015; Ding and Van Hoesen, 2015; Insausti and Amaral, 2004), while others separate them as their own individual subfields (Palomero-Gallagher et al., 2020; Rosene and Van Hoesen, 1987; Steve et al., 2017; Zilles et al., 2015). Additionally, the border between ParaSub and PreSub is often a source of disagreement: some authors suggest that PreSub contains the lamina principalis externa (LPE), which designates the border between the two subfields (Ding, 2013; Ding and Van Hoesen, 2015; Rosene and Van Hoesen, 1987), while others denote that the distinguishing feature is ParaSub's less defined lamina dessicans (cell free zone) compared to PreSub (Insausti et al., 2017; Zilles et al., 2015). These discrepancies, among others, could be due to using primarily qualitative approaches in subfield segmention. For example, several authors comment on neuronal sizes of various subfields qualitatively, but provide no quantitative evidence to support the descriptions (Ding, 2013; Ding and Van Hoesen, 2015; Insausti et al., 2017; Insausti and Amaral, 2004; Zilles et al., 2015). While using qualitative measures is an important tool in characterizing subfields, establishing quantitative measures that multiple inter-raters can reliably use provides essential ground truth data of the subfields.

The present study sought to obtain quantitative neuronal width measurements from the hippocampal subfields to provide a parcellation criterion to distinguish hippocampal subfields, and to determine ground truth hippocampal neuron size in the human brain. These quantitative measures will establish a baseline for this vulnerable circuit, and be applicable and useful for multiple diseases. We collected quantitative neuronal width measures in the individual hippocampal subfields (CA1-4, Sub, PreSub, ParaSub), as well as the uncinate (medial) subfields (CA1u-3u, Subu). Neuron width measurements were manually collected on pyramidal neurons in 18 human hippocampi. Further, measurements were collected on the hippocampal subfields at various anterior-posterior levels of the human hippocampus, which enabled us to compare neuron sizes within subfields across the full length of the hippocampus.

Methods

Tissue Samples

All 18 brain hemispheres were collected from the Massachusetts General Hospital Autopsy Service. Table 1 details demographic information for all cases. Brain samples were fixed by immersion with 10% formalin for at least two months. The ages ranged from 45–84 years with the mean 65.5 ± 11 years. The sex ratio was eight males, nine females, and one not available. Postmortem intervals before fixation were less than 24 hours with one exception (48 hours). The sample set included 13 left hemispheres and five right hemispheres, and brain weights ranged between 1060–1595 grams. Brain tissue was screened and diagnosed by a neuropathologist to control for comorbidities (MPF, SC, MLO). Tau antibody CP13 (gift from Dr. Peter Davies) was used to stage neurofibrillary tangle severity to assess Braak and Braak staging (MPF, JCA, JLR) (Braak et al., 2006; Braak and Braak, 1995, 1991). Table 1 shows the respective Braak and Braak stages, which were: five control cases, five Braak & Braak stage I cases, and eight Braak & Braak stage II cases. All cases included were preclinical stages of Braak's stages and did not report any cognitive nor memory impairment in their clinical history.

Table 1

Demographic information for all cases. Abbreviations include: Dx = diagnosis, F = female, M = male, N/A = not available, LH = Left Hemisphere, RH = Right Hemisphere, PMI = postmortem interval.

Case ID	Age	Sex	Hemisphere	Cause of death	PMI (hours)	Brain weight (grams)	Dx	Braak & Braak Stage
1	68	M	RH	Malignant mesothelioma	17	N/A	Cognitive control	NC
2	45	F	LH	Ischemic renal injury	24	1215	Cognitive control	NC
3	49	M	LH	Liver failure	3	1300	Cognitive control	NC
4	67	M	RH	Lung cancer	48	1380	Cognitive control	NC
5	45	F	LH	Lung disease	24	1411	Cognitive control	NC
6	70	F	LH	Cardiac arrest	23	1103	Cognitive control	BBI
7	79	M	LH	Surgery complications	15	1200	Cognitive control	BBI
8	59	M	LH	Liver failure	20	1319	Cognitive control	BBI
9	73	F	RH	Aortic dissection	23	1356	Cognitive control	BBI
10	68	M	RH	Acute cardiac death	24	1595	Cognitive control	BBI
11	N/A	N/A	LH	N/A	N/A	N/A	Cognitive control	BBII
12	73	F	LH	Visceral hemorrhage	24	1142	Cognitive control	BBII
13	60	M	RH	Liver failure	24	1166	Cognitive control	BBII
14	75	M	LH	Vascular disease	24	1187	Cognitive control	BBII
15	84	F	LH	Heart failure	24	1221	Cognitive control	BBII
16	60	F	LH	Pancreatic cancer	2	1328	Cognitive control	BBII

Case ID	Age	Sex	Hemisphere	Cause of death	PMI (hours)	Brain weight (grams)	Dx	Braak & Braak Stage
17	59	F	LH	Lung disease	24	1402	Cognitive control	BBII
18	74	F	LH	Coronary disease	24	1060	Cognitive control	BBII

Blocking & Sectioning Procedures

Hemispheres were stored in periodate-lysine-paraformaldehyde (PLP) at 4°C until ready to be blocked. Samples were blocked coronally in an orthogonal plane, perpendicular to the long axis of the hippocampus. The entire length of the hippocampus was included. Tissue was incubated in cryoprotectant (20% glycerol, 2% dimethyl sulfoxide) for at least 1 month prior to sectioning to ensure tissue was well protected. Medial temporal blocks were then serially sectioned in the coronal plane. We used a sliding freezing microtome (Leica SM2000R, Leica Biosystems Inc Buffalo Grove, IL) for sectioning at 50µm. Every section was saved sequentially and stored in cryoprotectant at -20ºC until staining experiments.

Histology

Medial temporal lobe tissue sections were rinsed free from cryoprotection, and hand mounted onto gel coated glass slides (gelatin, chromium potassium sulfate). Tissue that was mounted was selected at approximately every 10 sections; thus, mounted sections were separated by at least 500µm. Mounted tissue was dried overnight and underwent a Thionin Nissl stain (8% aqueous thionin, modified slightly from (Augustinack et al., 2005; Zilles et al., 2002). The Nissl stain protocol was as follows: tissue defatting (100% ethanol: chloroform [1:1 mixture]), soaked in 50% EtOH, rinsed in twice distilled water (ddH_2O), pretreated (acetic acid: acetone: ddH_2O: EtOH [1:1:1:1 mixture]), stained (8% aqueous thionin, sodium acetate stock, and acetic acid stock), and differentiated in 70% ethanol and a few drops of glacial acetic acid). The slides were then dehydrated in ethanol of ascending concentrations and cleared of water with xylene. Slides were coverslipped using Permount (Fisher Scientific, USA).

Slide Digitization and Visualization

All stained tissue were analyzed and evaluated using four microscopes: a Nikon80i (Microvideo Instruments, Avon MA), an Olympus BH-2 double headed microscope (Precise Instrument, Hansen MA), a Nikon SMZ1000 (Microvideo Instruments, Avon MA), and a Keyence digital microscope BZX800, (Keyence, Japan). The Nikon80i and Olympus BH-2 were used to evaluate the subfield architecture in depth and to identify the boundaries of the subfields, as described in the following section. The Olympus BH-2 is a double headed microscope, which allowed for inter-rater discussion during evaluation. Subfield boundaries were drawn in ultra-fine Sharpie marker under the Nikon SMZ1000 (EMW, JCA), and these parcellated slides were then digitized at 2x using the Keyence to keep record of drawn subfield

boundaries. Digitized images were imported into either Adobe Photoshop v2022 or GIMP 2.10.30 for further data analyses.

Subfield Parcellation Protocols and Analyses

Hippocampal Subfields

All subfield parcellations were done by two experts (EMW, JCA) to ensure accurate segmentation (Fig. 1, parcellated Nissl slide). Subfield parcellation was based primarily on the protocols defined in previous publications (Ding, 2013; Ding and Van Hoesen, 2015; Insausti et al., 2017; Insausti and Amaral, 2004; Rosene and Van Hoesen, 1987). CA1 is located on the dorsal most lateral edge as the lateral ventricle dips ventrally in the temporal lobe, and it contains the most lightly stained neurons of the CA fields. Both CA2 and CA3 contain neurons that stain darkly (i.e., chromophilic) and appear more densely packed than neurons in CA1. We differentiated CA2 and CA3 by their cellular organization. CA4 is located within the hilus region and has the least organized and least densely packed neurons of the CA fields. The subicular cortices (Sub, PreSub, and ParaSub) reside ventrally on the lower bank of the hippocampal sulcus. Sub differentiates from CA1 by the existence of the stratum radiatum in CA1 (Ding, 2013; Ding and Van Hoesen, 2015; Lorente de Nó, 1934), and by Sub's more tightly packed neurons than CA1. PreSub contains the presubicular clouds and the lateral principalis external (LPE) (Ding, 2013; Rosene and Van Hoesen, 1987), and is differentiated from ParaSub by its cellular organization.

Hippocampal Medial/Uncinate Subfields

The hippocampal head is much wider in the coronal plane than the hippocampal body and genu because the head contains the medial uncus, which has three gross morphological divisions (i.e., three small gyri or bulges): the gyrus uncinatus, the limbus Giacomini, and the gyrus intralimbicus (Gloor, 1997; Insausti and Amaral, 2004; ten Donkelaar et al., 2018). The gyrus uncinatus is the most rostral part, consisting primarily of the anterior most uncus and the hippocampal-amygdala transition area (HATA), which occurs dorsally to the uncus. The next bulge is the limbus Giacomini and contains the DG. Finally, the gyrus intralimbicus is the most caudal of the three external landmarks and contains the CA3 subfield. While these divisions annotate useful gross features, we chose to annotate in the coronal plane, and as such, refer to the medial area of the hippocampus as 'uncinate' regions and the lateral portion of the hippocampus as 'lateral' regions. This distinction clarifies regionality in the coronal stained section, provides greater detail, and eases readability. When the uncus is present in the hippocampus, multiple instances of the same subfield may appear in the same plane (Fig. 1). To accurately track the subfield location among subfield sites, we refer to the subfields in their lateral location as CA1, CA2, CA3, and the medial locations as CA1u (uncinate), CA2u, CA3u, and Subu. The uncinate subfields (CA1u, CA2u, CA3u, and Subu) equate to the uncal regions defined by Ding & Van Hoesen (2015) and Rosene & Van Hoesen (1987). These subfields share similar cytoarchitecture to their lateral counterparts, the only visual difference being the medial location.

Hippocampal Anterior – Posterior Levels

Related, but different from the gross subfield anatomy of the hippocampus described above, two structures (the hippocampal proper and the DG) intertwine, each with a unique cytoarchitecture, resulting in a complicated structure in cross-section. To best represent anatomical structures and subfields across the entirety of the hippocampus, we defined five coronal levels to investigate quantitatively. The five levels consist of *genu, pes, full DG, x-region, and body* (Fig. 2). *Genu* is the most anterior level and is relatively small (Fig. 2a). Moving posterior, hippocampal *pes* occurs once the hippocampal fissure has fully opened, and multiple pes appear dorsally (Fig. 2b). Notably, the DG is still posterior to this level. The next level is the *full DG*, wherein the DG is fully present and at its widest breath from medial to lateral (Fig. 2c). The *x-region*, coined by de Flores et al (2020), refers to the level where the DG has been split in two, and the pyramidal layer begins to separate into two disparate portions, yet still connected structurally (Fig. 2d). The pes, full DG and x-region all reside within the hippocampal head. Finally, the most posterior level is hippocampal *body*, where the hippocampal head/uncinate gyrus have ended (Fig. 2e). Only one level of the body was included due to the simplicity of that level; the body of the hippocampus does not undergo significant changes in appearance, compared to the hippocampal head.

Manual neuron width measurements

Systematic random sampling

Neuron width measurements were manually collected on all cases, using five Nissl-stained sections for each case, ensuring one slide was selected for each level. Pyramidal neurons were measured in the lateral subfields (CA1, CA2, CA3, CA4, Sub, PreSub, and ParaSub) as well as the medial subfields (CA1u, CA2u, CA3u, and Subu). PreSub and ParaSub neurons were measured in layer I, which contains the presubicular clouds and LPE; all other subfields were measured in layer II. The subfield parcellations on Nissl-stained slides were traced within the Stereoinvestigator software (v.2021.1.3, MicroBrightField Inc, Burlington VT) and categorized as regions of interest (ROIs) using the Nikon 80i and its 40x magnification (4x objective). EMW performed all neuron measurements. Ten neurons were measured per subregion per section, totaling 5,430 neurons measured among all cases. We employed a systematically random sampled protocol for neuronal selection, wherein the Stereoinvestigator software randomly placed 10–15 measurement frames within each subfield, similar to a counting grid. Counting (i.e., measurement) frames had two ‘inclusion’ lines (green) and two ‘exclusion’ lines (red). Pyramidal neurons were measured if they met these criteria: 1) its nucleus was visible and within the counting frame, but not touching the exclusion lines 2) its nucleolus was visible and 3) the neuron did not overlap with another neuron or glial cell. Neuron width measurements were manually collected at 200x magnification (20x objective). Given the differing sizes and three-dimensional nature of the subfields, some subfields were not present at all anterior-posterior levels. However, we always measured 10 neurons per subfield per level; this design was adopted to ensure that measurements could be compared across the same slide.

Feret’s diameter

We followed the principle of Feret's diameter to determine the width of the pyramidal neurons, as it is an ideal caliper measure for neuronal width (Arai, 1996; Merkus, 2009). The measurement line was drawn immediately inferior to the basal dendrites, at the widest part of the pyramidal neuron soma (Fig. 3). Neuronal width was measured rather than length or area because the apical dendrite was not always apparent, and the basal dendrites provided a more reliable landmark. The pyramidal neurons primarily appeared in three shapes, see Fig. 3 for examples for where line measurements were drawn.

Statistical analysis

Statistical analyses were performed and illustrated using both PyCharm CE 2020.2.3 and Prism v9.1 (GraphPad). Shapiro-Wilk tests were run to assess normality of data. A Kruskal-Wallis ANOVA test was used to test for group effects. Following a significant Kruskal-Wallis result, post-hoc analyses were conducted using Dunn's multiple comparisons tests. Mann-Whitney tests were used as the nonparametric independent t tests. Spearman correlations were used to assess correlations between neuron size and other variables, such as age and Braak & Braak stage. The significance level was set at $p < 0.05$.

Results

Neuron Width Measurements for Lateral and Medial Subfields

Table 2
lists the means, medians, standard deviation (STD) standard error of the mean (S.E.M), and confidence intervals (CI) of the neuronal measurements for all subfields. A Kruskal-Wallis test revealed a highly significant subfield effect on neuron size ($p < 0.0001$). Further, multiple comparisons showed the differences in neuron size among each subfield. Figure 4 shows the neuron width measurements for the lateral hippocampal proper subfields (CA1-4). Subfield CA1 revealed the smallest neurons among the CA fields. Significant neuron size differences were observed between CA1 and CA2, CA1 and CA3, and CA1 and CA4 (all $p < 0.0001$). Neurons in CA4 were significantly larger than neurons in CA3 ($p = 0.0009$). No significant neuron size differences were found between subfields CA2 and CA3, CA2 and CA4, or Sub and CA1 (all $p > 0.999$). Figure 4b illustrates the neuron width measurements for the subicular cortices (Sub, PreSub, and ParaSub). Both ParaSub neurons and PreSub neurons were significantly smaller than neurons in Sub (both $p < 0.0001$), and the neurons in PreSub were significantly smaller than the neurons in ParaSub ($p = 0.0003$).

Region	n	Mean (µm)	Median (µm)	STD (µm)	S.E.M. (µm)	CI (µm)
CA1	880	15.36	15.31	1.66	0.06	[15.25, 15.47]
CA1U	200	14.62	14.45	1.83	0.13	[14.37, 14.88]
CA2	530	16.80	16.75	1.81	0.08	[16.64, 16.95]
CA2U	200	14.63	14.80	1.73	0.12	[14.39, 14.87]
CA3	510	16.36	16.41	1.77	0.08	[16.21, 16.51]
CA3U	150	14.97	14.78	1.49	0.12	[14.73, 15.21]
CA4	360	17.35	17.34	2.00	0.11	[17.15, 17.56]
Sub	880	15.51	15.48	1.67	0.06	[15.40, 15.62]
SubU	380	14.76	14.76	1.78	0.09	[14.58, 14.94]
PreSub*	750	8.01	7.94	1.14	0.04	[7.93, 8.09]
ParaSub*	590	9.42	9.26	1.46	0.06	[9.30, 9.54]

Table 2. Descriptive statistics for neurons (n) measured, mean, median, standard deviation (STD), standard error of mean (S.E.M.), and confidence intervals (CI, 95%) for each subfield. Asterisk (*) denotes measurements were from LPE and not from the pyramidal cell layer.

Figure 4c displays the hippocampal medial-lateral location effects on neuron size. Our data demonstrate that every lateral hippocampal subfield was larger than its medial counterpart (Fig. 3D). More specifically, neuron width measurements of CA1 neurons were larger than neurons in CA1u ($p = 0.0147$), CA2 neurons were larger than CA2u neurons ($p < 0.0001$), and CA3 neurons were larger than CA3u neurons ($p < 0.0001$). The subiculum continued this pattern as neurons in lateral subiculum were larger than those in the medial counterpart, Subu ($p < 0.0001$). In addition, contrary to their lateral counterparts, which showed differences among each other (Fig. 4a & 4b), no significant differences were found among any of the

medial subfields for neuron width measurements (all $p > 0.999$). For example, CA1u and CA2u did not differ from each other in size, CA2u did not differ from CA3u, and so on.

Variables: Hemisphere, case, anterior-posterior levels, and age

Hemisphere

We evaluated whether laterality affected neuron size in our sample set. The laterality test was assessed in male samples (n = 8) only, since we did not have an equal number of female cases for left and right hemispheres A Mann-Whitney test revealed a significant difference among neuron sizes collected in right hemisphere (n = 4) and those collected in left hemisphere (n = 4), such that neurons in left hippocampi were smaller than those in right hippocampi (males, $p < 0.0001$) (Fig. 5). Sex as an effect was not evaluated given the sample set was unequal for the number of males and females per hemisphere.

Case

A Kruskal-Wallis test determined that there was a main effect of case on neuron size ($p < 0.0001$). Multiple comparisons revealed that four cases (Cases 3, 5, 7, and 8) had significantly smaller neurons from multiple other cases (Fig. 6).

Anterior-Posterior Levels

To determine whether neuronal sizes depended on the anterior-posterior level of the hippocampus, we evaluated neuron size in CA1 and Sub. Subregions CA1 and Sub were selected since these subfields appear at every level of the hippocampus; other subfields only appear at certain levels. A Kruskal-Wallis test revealed no significant differences in neuronal size for CA1 across the five levels ($p = 0.16$), nor Sub across the five levels ($p = 0.55$). Thus, neuron size does not differ given the anterior-posterior level.

Age, Diagnosis

We also compared age and neuron size for all subfields but observed no correlation between them (Spearman correlation, $r = 0.28$, $p = 0.38$). Notably, the ages (45–84) in this sample set were restricted to middle age and older adults but did not include any considerably older adults (85+). We also compared diagnosis against neuron size and observed that normal controls (NC) had significantly larger neurons than BBI cases ($p < 0.0001$). No difference was found between NC and BBII neuron sizes ($p = 0.2494$). BBI cases were found to have significantly smaller neurons than BBII cases ($p = 0.0044$) and thus neuron sizes ranked as NC = BBII > BBI. To determine if Braak & Braak staging, regardless of I or II, significantly varied in neuron sizes from controls, we ran a Mann-Whitney test which revealed that controls had significantly larger neurons than Braak & Braak stages combined ($p = 0.0014$).

Discussion

The major findings in this study were the differences in neuron widths among the CA fields and the diverse neuron widths within the subicular cortices. Among the CA fields, we found that CA1 had the smallest neurons, but no difference was observed between CA2 and CA3. Further, CA4 neurons were larger than CA3 neurons. CA1 and Sub neurons were the same size. Our measurements indicate that Sub had the largest neurons of the subicular cortices, and that ParaSub had larger neurons than PreSub. We summarize the pyramidal neuron size in each respective subfield is as follows CA4 > CA3 = CA2 > CA1 = Sub > ParaSub > PreSub. We found significant differences in neuron sizes between lateral subfields and their medial (uncinate) counterparts. Finally, we found significant differences in neuron sizes between left and right hemispheres, and between cognitive controls and Braak & Braak stages I and II.

Our findings confirm, clarify, and expand on the existing qualitative reports. For instance, we corroborate reports that describe CA1 has smaller neurons than CA2 (Ding and Van Hoesen, 2015; Insausti and Amaral, 2004), and that ParaSub has larger neurons than PreSub (Ding and Van Hoesen, 2015). Additionally, we clarify other differences in the CA fields. Some reports have disagreed about whether subfield CA4 exists (de Flores et al., 2015; Ding and Van Hoesen, 2015; Insausti and Amaral, 2004), but our findings show that CA4 has larger neurons than CA3. Thus, coupled with the location of CA4 inside the hilus and its modified pyramidal neurons, we present strong evidence for a clear separation of CA3 and CA4 as two subfields. Lastly, our findings expand on the existing qualitative remarks on certain subfields and add quantitative measures on all subregions in the hippocampus. Notably, previous reports remark on neuron size in a particular subfield but do not provide quantitative comparison to its neighboring subfield. For example, it has been described previously that CA3 has “large neurons”, but the reports do not state whether CA3 neurons are larger than its immediate neighbors CA2 or CA4 (Ding and Van Hoesen, 2015; Rosene and Van Hoesen, 1987). Our findings indicate that CA3 has smaller neurons than CA4, but similar neuron sizes to CA2. As such, our data provides quantifiable markers on the exact location of the CA3/CA4 boundary. Our results indicate no significant difference between CA1 and Sub, although a qualitative report that Sub has larger neurons than CA1 (Insausti and Amaral, 2004). Often times, the criteria to distinguish the CA1/Sub boundary is that Sub has no stratum radiatum (Ding, 2013; Ding and Van Hoesen, 2015; Lorente de Nó, 1934; Rosene and Van Hoesen, 1987). However, the stratum radiatum does not stain well in *all* human tissue preparations and thus is a less reliable feature for segmentation purposes. This, and the lack of quantifiable differences in neuron sizes between CA1 and Sub reported here illustrate a need for additional identifiers to parcellate these two subfields. In sum, our quantitative results provide segmentation guidance for most but not all subfields.

A novel finding in this report pertains to neuron size in the medial hippocampal subfields: CA1u, CA2u, CA3u, and Subu. We found that each medial subfield has smaller neurons than its lateral subfield (CA1 versus CA1u, CA2 versus CA2u, and so on). However, we observed no neuronal width differences among the medial subfields (CA1u, CA2u, CA3u, Subu). For example, we did not observe any neuron size differences between CA1u and CA2u, as was observed between lateral CA1 and CA2. It could be argued, then, that based on neuron sizes, CA1u, CA2u, and CA3u represent unique subfields from their lateral counterpart. However, we advocate that quantitative and qualitative differences should be used in tandem to establish subfield boundaries. As such, the qualitative similarities (as outlined in Ding & Van

Hoesen (2015)), between CA1 and CA1u, CA2 and CA2u, and so on, indicate that these subfields indeed represent the same subfields, but their neuron sizes differ depending on their medial-lateral location. Connectivity differences between the uncinate and lateral subfields may explain these neuron size differences. For instance, the uncus is thought to mediate the communication between the hippocampus and the prefrontal cortex (Zeidman and Maguire, 2016). Further, in fMRI experiments the uncus has been shown to engage when participates were asked to recall scenes that occurred a week prior, suggesting that the uncus has a distinct function from the lateral area of the hippocampus (Zeidman et al., 2015). However, the uncus is vastly understudied in both histology and neuroimaging reports, so it is difficult to draw conclusions at this time.

We also observed that the right hippocampus had significantly larger neurons than the left hippocampus. MRI studies have consistently found that the right hippocampus is greater in volume than the left hippocampus (Pedraza et al., 2004; Sarica et al., 2018). Our finding suggests that hippocampal neuron size may be responsible for and may correlate with the volume of the hippocampus. This presumptive correlation between neuron sizes and hippocampal volume has been supported by the findings that depression and schizophrenia reduce both hippocampal volume (Bremner et al., 2000; Harrison, 2004) and hippocampal neuron sizes (Stockmeier et al., 2004; Zaidel et al., 1997). While human hippocampal neuron size changes have not yet been explored in Alzheimer's disease, it has been shown that Alzheimer's disease does result in a reduced hippocampal volume (Du, 2001; Schuff et al., 2009; Shi et al., 2009). Presently, we explored whether neuron size differs in aging and preclinical Alzheimer's stages (Braak & Braak stages I and II), but still cognitive controls. We found that Braak & Braak I cases had the smallest neurons compared to controls and Braak & Braak II cases, but no difference was found between controls and Braak & Braak II cases. We expected that both Braak & Braak I and II cases would have smaller neurons than our control brains, but this was not the case. This could be due to the inclusion of only preclinical, early Braak & Braak stages, which are still classified as cognitive controls. Our findings suggests that if neuron size is impacted by Alzheimer's disease, it does so at a later stage.

In general, neuron size reports have been limited, especially within the human hippocampus. In the schizophrenia literature, some reports have provided size differences, using neuron area, within the CA fields between control and schizophrenic patients at the level of the hippocampal body (Arnold et al., 1995; Benes et al., 1991; Jönsson et al., 1999; Todtenkopf and Benes, 1998; Zaidel et al., 1997). We discern four noteworthy differences between the previous works and our findings. First, while these studies provide valuable insight into the neuron sizes of the hippocampus, their studies centered on comparing neuron sizes between cognitively healthy controls and schizophrenic brains. For example, these reports compared CA1 neuron sizes between controls and schizophrenic patients, rather than comparing CA1 and CA2. While this was best for their aims, our focus was instead on comparing neuron sizes among subfields for parcellation purposes, and we only included cognitive controls. Second, these reports typically examined neuron sizes only in CA1-4, and only one included subiculum (Arnold et al., 1995); measurements from ParaSub, PreSub, or any medial CA subfields were not collected previously. Third, the measurements were collected from one level, the hippocampal body. Collecting neuron measurements from the subfields at various levels provides an anatomical context to the neuron size

findings and is an innovative approach that may provide valuable data to the neuroimaging community. Several studies have begun to evaluate the anterior-posterior aspect of the hippocampus and have shown differences in function and connectivity among the different levels (Malykhin N et al 2017; Gordon et al 2013 and Ta 2011). Thus, it is important to understand where, if at all, neuron sizes differ depending on anterior-posterior location in the hippocampus. Fourth, the mean area of each subfield varied immensely among reports. For instance, Benes and colleagues reported the CA1 neurons with a mean area of 559.2 μm^2 (Benes et al., 1991), and Jönsson et al reported mean CA1 neurons at 353.4 μm^2 (Jönsson et al., 1999). This substantial variability in neuron sizes between the studies could be due to each study's defining criteria and methods, such as including the axons/dendrites when outlining a neuron and/or not having the most accurate subfield parcellations. Thus, we chose to measure neuronal width rather than area so that subjective biases can be minimized – that is, axons and dendrites were not included. While these previous reports were first to provide hippocampal neuron size data, we expanded on their work by measuring and comparing neuron sizes among all the hippocampal subfields and subicular cortices, collecting these measurements at multiple anterior-posterior levels, and by using an unbiased sampling method using a consistent measure (Feret's diameter).

Multiple fields within neuroscience rely on accurate and reliable segmentations of the hippocampus. We speculate that disagreement and/or confusion exists in subfield parcellations due to the use of primarily qualitative observations. This controversary can be problematic since many of the *ex vivo* MRI atlases base their segmentations on these parcellations (Adler et al., 2018; Iglesias et al., 2015; Olsen et al., 2019; Parekh et al., 2015; Wisse et al., 2017; Yushkevich et al., 2015, 2009). *In vivo* MRI has poor resolution, which makes segmentation increasingly difficult, often leading to some authors basing their subfield boundaries on angles or extrapolations (Bender et al., 2017; Mueller et al., 2007; Raz et al., 2015). Qualitative observations serve an excellent purpose, but when one must draw a definitive cytoarchitectural boundary line at the microscopic scale, using both quantitative markers and qualitative markers is most reliable and lends more compelling evidence.

We denote multiple strengths in this report, including the large number of neurons (n = 5430) measured, the inclusion of both lateral and medial subfields, and collecting measurements from multiple anterior-posterior levels. Our findings on neurons manually measured neurons provide a strong foundational understanding of the subfields' neuronal sizes. The subfields included were the subicular cortices (ParaSub, PreSub, Sub) inferiorly, the lateral subfields dorsally (CA1, CA2, CA3, CA4) and the uncinate regions medially (CA1u, CA2u, CA3u). The inclusion of the medial subfields provides context to how subfields may change depending on its medial-lateral axis of the hippocampus. Notably, we also provide data on ParaSub and PreSub, two subfields consistently not included in the existing neuron measurement data within the previously noted schizophrenia studies, and routinely not included in *in vivo* parcellations. Finally, we report neuron sizes from multiple anterior-posterior levels, which gives a comprehensive view and expands on the existing neuron size reports. Thus, our thorough sampling of the hippocampus provides novel data on the uncinate (medial) area of the hippocampal head, as well as multiple coronal levels, two aspects that are often overlooked.

While this report has notable strengths, it is not without limitations; specifically, we note three minor limitations. First, we did not include prosubiculum because it is currently widely debated as to whether prosubiculum is present, and related, the neuroanatomy field lacks an understanding of prosubiculum's appearance. Second, the inclusion of samples that have Braak & Braak stage I and II and light tau pathology in the perirhinal and entorhinal cortices. However, the cases had no clinical memory symptoms and had only isolated neurofibrillary tangles (one or two tangles at most) in the hippocampal regions, so we consider this a relatively minor limitation. Moreover, we found no effect of diagnosis on neuron size, which also suggests that this is a minor limitation. Finally, although we had a good sample size, n = 18 cases for general analyses, this number significantly falls when we separate variables (sex, hemisphere, and diagnosis). While findings showed a strong and significant effect for the analyses we ran for hemisphere and diagnoses, future studies will need to confirm our findings. Future studies will also need to explore the neuronal width differences between the sexes, as we did not have enough female brains to run such an analysis.

Declarations

Acknowledgements

Grant support for this research was provided by the National Institute of Health: R01AG057672 and RF1AG072056. We are grateful for Dr. Peter Davies for tau antibody gift (CP13), and we appreciate his generosity and kindness over the years. We thank the brain donors and their families for their generous support, for without them this research would not be possible.

Funding

Grant support for this research was provided by the National Institute of Health: R01AG057672 and RF1AG072056.

Conflict of interests

We have no conflict of interests to report.

Data availability statement

The full data set collected for this manuscript is available from the corresponding author upon reasonable request.

Author Contributions

All authors contributed to the study conception, design, and material preparation. Data collection and analysis were performed by Emily Williams and Josue Llamas-Rodriguez. The first draft of the manuscript was written by Emily Williams and all authors commented on previous versions of the manuscript. All authors read and approved the final manuscript.

References

Adler, D.H., Pluta, J., Kadivar, S., Craige, C., Gee, J.C., Avants, B.B., Yushkevich, P.A., 2014. Histology-derived volumetric annotation of the human hippocampal subfields in postmortem MRI. NeuroImage 84, 10.1016/j.neuroimage.2013.08.067. https://doi.org/10.1016/j.neuroimage.2013.08.067

Adler, D.H., Wisse, L.E.M., Ittyerah, R., Pluta, J.B., Ding, S.-L., Xie, L., Wang, J., Kadivar, S., Robinson, J.L., Schuck, T., Trojanowski, J.Q., Grossman, M., Detre, J.A., Elliott, M.A., Toledo, J.B., Liu, W., Pickup, S., Miller, M.I., Das, S.R., Wolk, D.A., Yushkevich, P.A., 2018. Characterizing the human hippocampus in aging and Alzheimer's disease using a computational atlas derived from ex vivo MRI and histology. Proc. Natl. Acad. Sci. U. S. A. 115, 4252–4257. https://doi.org/10.1073/pnas.1801093115

Arai, Y., 1996. Chemistry of Powder Production. Springer Science & Business Media.

Arnold, S.E., Franz, B.R., Gur, R.C., Gur, R.E., Shapiro, R.M., Moberg, P.J., Trojanowski, J.Q., 1995. Smaller neuron size in schizophrenia in hippocampal subfields that mediate cortical-hippocampal interactions. Am. J. Psychiatry 152, 738–748. https://doi.org/10.1176/ajp.152.5.738

Augustinack, J.C., van der Kouwe, A.J.W., Blackwell, M.L., Salat, D.H., Wiggins, C.J., Frosch, M.P., Wiggins, G.C., Potthast, A., Wald, L.L., Fischl, B.R., 2005. Detection of Entorhinal Layer II Using Tesla Magnetic Resonance Imaging. Ann. Neurol. 57, 10.1002/ana.20426. https://doi.org/10.1002/ana.20426

Bender, A.R., Keresztes, A., Bodammer, N.C., Shing, Y.L., Werkle-Bergner, M., Daugherty, A.M., Yu, Q., Kühn, S., Lindenberger, U., Raz, N., 2017. Optimization and validation of automated hippocampal subfield segmentation across the lifespan. Hum. Brain Mapp. 39, 916–931. https://doi.org/10.1002/hbm.23891

Benes, F.M., Sorensen, I., Bird, E.D., 1991. Reduced Neuronal Size in Posterior Hippocampus of Schizophrenic Patients. Schizophr. Bull. 17, 597–608. https://doi.org/10.1093/schbul/17.4.597

Boccardi, M., Bocchetta, M., Apostolova, L.G., Barnes, J., Bartzokis, G., Corbetta, G., DeCarli, C., deToledo-Morrell, L., Firbank, M., Ganzola, R., Gerritsen, L., Henneman, W., Killiany, R.J., Malykhin, N., Pasqualetti, P., Pruessner, J.C., Redolfi, A., Robitaille, N., Soininen, H., Tolomeo, D., Wang, L., Watson, C., Wolf, H., Duvernoy, H., Duchesne, S., Jack, C.R., Frisoni, G.B., 2015. Delphi definition of the EADC-ADNI Harmonized Protocol for hippocampal segmentation on magnetic resonance. Alzheimers Dement. J. Alzheimers Assoc. 11, 126–138. https://doi.org/10.1016/j.jalz.2014.02.009

Bonne, O., Vythilingam, M., Inagaki, M., Wood, S., Neumeister, A., Nugent, A.C., Snow, J., Luckenbaugh, D.A., Bain, E.E., Drevets, W.C., Charney, D.S., 2008. Reduced Posterior Hippocampal Volume in Posttraumatic Stress Disorder. J. Clin. Psychiatry 69, 1087–1091.

Bosco, P., Redolfi, A., Bocchetta, M., Ferrari, C., Mega, A., Galluzzi, S., Austin, M., Chincarini, A., Collins, D.L., Duchesne, S., Maréchal, B., Roche, A., Sensi, F., Wolz, R., Alegret, M., Assal, F., Balasa, M., Bastin, C., Bougea, A., Emek-Savaş, D.D., Engelborghs, S., Grimmer, T., Grosu, G., Kramberger, M.G., Lawlor, B., Mandic

Stojmenovic, G., Marinescu, M., Mecocci, P., Molinuevo, J.L., Morais, R., Niemantsverdriet, E., Nobili, F., Ntovas, K., O'Dwyer, S., Paraskevas, G.P., Pelini, L., Picco, A., Salmon, E., Santana, I., Sotolongo-Grau, O., Spiru, L., Stefanova, E., Popovic, K.S., Tsolaki, M., Yener, G.G., Zekry, D., Frisoni, G.B., 2017. The impact of automated hippocampal volumetry on diagnostic confidence in patients with suspected Alzheimer's disease: A European Alzheimer's Disease Consortium study. Alzheimers Dement. J. Alzheimers Assoc. 13, 1013–1023. https://doi.org/10.1016/j.jalz.2017.01.019

Braak, H., Alafuzoff, I., Arzberger, T., Kretzschmar, H., Del Tredici, K., 2006. Staging of Alzheimer disease-associated neurofibrillary pathology using paraffin sections and immunocytochemistry. Acta Neuropathol. (Berl.) 112, 389–404. https://doi.org/10.1007/s00401-006-0127-z

Braak, H., Braak, E., 1995. Staging of Alzheimer's disease-related neurofibrillary changes. Neurobiol. Aging 16, 271–278; discussion 278-284. https://doi.org/10.1016/0197-4580(95)00021-6

Braak, H., Braak, E., 1991. Neuropathological stageing of Alzheimer-related changes. Acta Neuropathol. (Berl.) 82, 239–259. https://doi.org/10.1007/BF00308809

Bremner, J.D., Narayan, M., Anderson, E.R., Staib, L.H., Miller, H.L., Charney, D.S., 2000. Hippocampal Volume Reduction in Major Depression. Am. J. Psychiatry 157, 115–118. https://doi.org/10.1176/ajp.157.1.115

Buzsáki, G., Moser, E.I., 2013. Memory, navigation and theta rhythm in the hippocampal-entorhinal system. Nat. Neurosci. 16, 130–138. https://doi.org/10.1038/nn.3304

Dam, A.M., 1980. Epilepsy and Neuron Loss in the Hippocampus. Epilepsia 21, 617–629. https://doi.org/10.1111/j.1528-1157.1980.tb04315.x

de Flores, R., Berron, D., Ding, S.-L., Ittyerah, R., Pluta, J.B., Xie, L., Adler, D.H., Robinson, J.L., Schuck, T., Trojanowski, J.Q., Grossman, M., Liu, W., Pickup, S., Das, S.R., Wolk, D.A., Yushkevich, P.A., Wisse, L.E.M., 2020. Characterization of hippocampal subfields using ex vivo MRI and histology data: lessons for in vivo segmentation. Hippocampus 30, 545–564. https://doi.org/10.1002/hipo.23172

de Flores, R., La Joie, R., Chételat, G., 2015. Structural imaging of hippocampal subfields in healthy aging and Alzheimer's disease. Neuroscience 309, 29–50. https://doi.org/10.1016/j.neuroscience.2015.08.033

de Lanerolle, N.C., Kim, J.H., Robbins, R.J., Spencer, D.D., 1989. Hippocampal interneuron loss and plasticity in human temporal lobe epilepsy. Brain Res. 495, 387–395. https://doi.org/10.1016/0006-8993(89)90234-5

Ding, S.-L., 2013. Comparative anatomy of the prosubiculum, subiculum, presubiculum, postsubiculum, and parasubiculum in human, monkey, and rodent. J. Comp. Neurol. 521, 4145–4162. https://doi.org/10.1002/cne.23416

Ding, S.-L., Van Hoesen, G.W., 2015. Organization and Detailed Parcellation of Human Hippocampal Head and Body Regions Based on a Combined Analysis of Cyto- and Chemoarchitecture. J. Comp. Neurol. 523, 2233–2253. https://doi.org/10.1002/cne.23786

Du, A.T., 2001. Magnetic resonance imaging of the entorhinal cortex and hippocampus in mild cognitive impairment and Alzheimer's disease. J. Neurol. Neurosurg. Psychiatry 71, 441–447. https://doi.org/10.1136/jnnp.71.4.441

Duvernoy, H.M., 2005. The Human Hippocampus: Functional Anatomy, Vascularization and Serial Sections with MRI. Springer Science & Business Media.

Engel, J., 1996. Introduction to temporal lobe epilepsy. Epilepsy Res., Mechanisms of Chronic Models of Epilepsy 26, 141–150. https://doi.org/10.1016/S0920-1211(96)00043-5

Frisoni, G.B., Jack, C.R., 2011. Harmonization of magnetic resonance-based manual hippocampal segmentation: a mandatory step for wide clinical use. Alzheimers Dement. J. Alzheimers Assoc. 7, 171–174. https://doi.org/10.1016/j.jalz.2010.06.007

Gloor, P., 1997. The temporal lobe and limbic system. Oxford Press, New York.

Goubran, M., Bernhardt, B.C., Cantor-Rivera, D., Lau, J.C., Blinston, C., Hammond, R.R., de Ribaupierre, S., Burneo, J.G., Mirsattari, S.M., Steven, D.A., Parrent, A.G., Bernasconi, A., Bernasconi, N., Peters, T.M., Khan, A.R., 2015. In vivo MRI signatures of hippocampal subfield pathology in intractable epilepsy. Hum. Brain Mapp. 37, 1103–1119. https://doi.org/10.1002/hbm.23090

Hannula, D.E., Tranel, D., Cohen, N.J., 2006. The long and the short of it: relational memory impairments in amnesia, even at short lags. J. Neurosci. Off. J. Soc. Neurosci. 26, 8352–8359. https://doi.org/10.1523/JNEUROSCI.5222-05.2006

Harnett, N.G., Goodman, A.M., Knight, D.C., 2020. PTSD-related neuroimaging abnormalities in brain function, structure, and biochemistry. Exp. Neurol. 330, 113331. https://doi.org/10.1016/j.expneurol.2020.113331

Harrison, P.J., 2004. The hippocampus in schizophrenia: a review of the neuropathological evidence and its pathophysiological implications. Psychopharmacology (Berl.) 174, 151–162. https://doi.org/10.1007/s00213-003-1761-y

Heckers, S., Rauch, S., Goff, D., Savage, C., Schacter, D., Fischman, A., Alpert, N., 1998. Impaired recruitment of the hippocampus during conscious recollection in schizophrenia. Nat. Neurosci. 1, 318–323. https://doi.org/10.1038/1137

Iglesias, J.E., Augustinack, J.C., Nguyen, K., Player, C.M., Player, A., Wright, M., Roy, N., Frosch, M.P., McKee, A.C., Wald, L.L., Fischl, B., Van Leemput, K., 2015. A computational atlas of the hippocampal formation

using ex vivo, ultra-high resolution MRI: Application to adaptive segmentation of in vivo MRI. NeuroImage 115, 117–137. https://doi.org/10.1016/j.neuroimage.2015.04.042

Insausti, R., Amaral, D., 2004. Hippocampal Formation, in: The Human Nervous System, Second Addition. pp. 871–914.

Insausti, R., Muñoz-López, M., Insausti, A.M., Artacho-Pérula, E., 2017. The Human Periallocortex: Layer Pattern in Presubiculum, Parasubiculum and Entorhinal Cortex. A Review. Front. Neuroanat. 11, 84. https://doi.org/10.3389/fnana.2017.00084

Jaroudi, W., Garami, J., Garrido, S., Hornberger, M., Keri, S., Moustafa, A.A., 2017. Factors underlying cognitive decline in old age and Alzheimer's disease: the role of the hippocampus. Rev. Neurosci. 28, 705–714. https://doi.org/10.1515/revneuro-2016-0086

Jönsson, S.A., Luts, A., Guldberg-Kjaer, N., Ohman, R., 1999. Pyramidal neuron size in the hippocampus of schizophrenics correlates with total cell count and degree of cell disarray. Eur. Arch. Psychiatry Clin. Neurosci. 249, 169–173. https://doi.org/10.1007/s004060050083

Logue, M.W., van Rooij, S.J.H., Dennis, E.L., Davis, S.L., Hayes, J.P., Stevens, J.S., Densmore, M., Haswell, C.C., Ipser, J., Koch, S.B.J., Korgaonkar, M., Lebois, L.A.M., Peverill, M., Baker, J.T., Boedhoe, P.S.W., Frijling, J.L., Gruber, S.A., Harpaz-Rotem, I., Jahanshad, N., Koopowitz, S., Levy, I., Nawijn, L., O'Connor, L., Olff, M., Salat, D.H., Sheridan, M.A., Spielberg, J.M., van Zuiden, M., Winternitz, S.R., Wolff, J.D., Wolf, E.J., Wang, X., Wrocklage, K., Abdallah, C.G., Bryant, R.A., Geuze, E., Jovanovic, T., Kaufman, M.L., King, A.P., Krystal, J.H., Lagopoulos, J., Bennett, M., Lanius, R., Liberzon, I., McGlinchey, R.E., McLaughlin, K.A., Milberg, W.P., Miller, M.W., Ressler, K.J., Veltman, D.J., Stein, D.J., Thomaes, K., Thompson, P.M., Morey, R.A., 2018. Smaller Hippocampal Volume in Posttraumatic Stress Disorder: A Multisite ENIGMA-PGC Study: Subcortical Volumetry Results From Posttraumatic Stress Disorder Consortia. Biol. Psychiatry 83, 244–253. https://doi.org/10.1016/j.biopsych.2017.09.006

Lorente de Nó, R., 1934. Studies on the structure of the cerebral cortex. II. Continuation of the study of the ammonic system. J. Für Psychol. Neurol. 46, 113–177.

Merkus, H.G., 2009. Particle Size, Size Distributions and Shape, in: Merkus, H.G. (Ed.), Particle Size Measurements: Fundamentals, Practice, Quality, Particle Technology Series. Springer Netherlands, Dordrecht, pp. 13–42. https://doi.org/10.1007/978-1-4020-9016-5_2

Mueller, S.G., Stables, L., Du, A.T., Schuff, N., Truran, D., Cashdollar, N., Weiner, M.W., 2007. Measurement of hippocampal subfields and age-related changes with high resolution MRI at 4 T. Neurobiol. Aging 28, 719–726. https://doi.org/10.1016/j.neurobiolaging.2006.03.007

O'Keefe, J., Burgess, N., Donnett, J.G., Jeffery, K.J., Maguire, E.A., 1998. Place cells, navigational accuracy, and the human hippocampus. Philos. Trans. R. Soc. B Biol. Sci. 353, 1333–1340.

Olsen, R.K., Carr, V.A., Daugherty, A.M., La Joie, R., Amaral, R.S.C., Amunts, K., Augustinack, J.C., Bakker, A., Bender, A.R., Berron, D., Boccardi, M., Bocchetta, M., Burggren, A.C., Chakravarty, M.M., Chételat, G., de Flores, R., DeKraker, J., Ding, S.-L., Geerlings, M.I., Huang, Y., Insausti, R., Johnson, E.G., Kanel, P., Kedo, O., Kennedy, K.M., Keresztes, A., Lee, J.K., Lindenberger, U., Mueller, S.G., Mulligan, E.M., Ofen, N., Palombo, D.J., Pasquini, L., Pluta, J., Raz, N., Rodrigue, K.M., Schlichting, M.L., Lee Shing, Y., Stark, C.E.L., Steve, T.A., Suthana, N.A., Wang, L., Werkle-Bergner, M., Yushkevich, P.A., Yu, Q., Wisse, L.E.M., Hippocampal Subfields Group, 2019. Progress update from the hippocampal subfields group. Alzheimers Dement. Amst. Neth. 11, 439–449. https://doi.org/10.1016/j.dadm.2019.04.001

Palomero-Gallagher, N., Kedo, O., Mohlberg, H., Zilles, K., Amunts, K., 2020. Multimodal mapping and analysis of the cyto- and receptorarchitecture of the human hippocampus. Brain Struct. Funct. 225, 881–907. https://doi.org/10.1007/s00429-019-02022-4

Pan, N., Zheng, K., Zhao, Y., Zhang, D., Dong, C., Xu, J., Li, X., Zheng, Y., 2021. Morphometry Difference of the Hippocampal Formation Between Blind and Sighted Individuals. Front. Neurosci. 15, 715749. https://doi.org/10.3389/fnins.2021.715749

Parekh, M.B., Rutt, B.K., Purcell, R., Chen, Y., Zeineh, M.M., 2015. Ultra-high Resolution In-vivo 7.0T Structural Imaging of the Human Hippocampus Reveals the Endfolial Pathway. NeuroImage 112, 1–6. https://doi.org/10.1016/j.neuroimage.2015.02.029

Pedraza, O., Bowers, D., Gilmore, R., 2004. Asymmetry of the hippocampus and amygdala in MRI volumetric measurements of normal adults. J. Int. Neuropsychol. Soc. JINS 10, 664–678. https://doi.org/10.1017/S1355617704105080

Raz, N., Daugherty, A.M., Bender, A.R., Dahle, C.L., Land, S., 2015. Volume of the Hippocampal Subfields in Healthy Adults: Differential Associations with Age and a Pro-inflammatory Genetic Variant. Brain Struct. Funct. 220, 2663–2674. https://doi.org/10.1007/s00429-014-0817-6

Rosene, D.L., Van Hoesen, G.W., 1987. The Hippocampal Formation of the Primate Brain, in: Jones, E.G., Peters, A. (Eds.), Cerebral Cortex: Further Aspects of Cortical Function, Including Hippocampus, Cerebral Cortex. Springer US, Boston, MA, pp. 345–456. https://doi.org/10.1007/978-1-4615-6616-8_9

Rubin, R.D., Watson, P.D., Duff, M.C., Cohen, N.J., 2014. The role of the hippocampus in flexible cognition and social behavior. Front. Hum. Neurosci. 8.

Sarica, A., Vasta, R., Novellino, F., Vaccaro, M.G., Cerasa, A., Quattrone, A., The Alzheimer's Disease Neuroimaging Initiative, 2018. MRI Asymmetry Index of Hippocampal Subfields Increases Through the Continuum From the Mild Cognitive Impairment to the Alzheimer's Disease. Front. Neurosci. 12.

Schuff, N., Woerner, N., Boreta, L., Kornfield, T., Shaw, L.M., Trojanowski, J.Q., Thompson, P.M., Jack, C.R., Weiner, M.W., 2009. MRI of hippocampal volume loss in early Alzheimer's disease in relation to ApoE genotype and biomarkers. Brain 132, 1067–1077. https://doi.org/10.1093/brain/awp007

Shi, F., Liu, B., Zhou, Y., Yu, C., Jiang, T., 2009. Hippocampal volume and asymmetry in mild cognitive impairment and Alzheimer's disease: Meta-analyses of MRI studies. Hippocampus 19, 1055–1064. https://doi.org/10.1002/hipo.20573

Squire, L.R., 2004. Memory systems of the brain: A brief history and current perspective. Neurobiol. Learn. Mem., Multiple Memory Systems 82, 171–177. https://doi.org/10.1016/j.nlm.2004.06.005

Steve, T.A., Yasuda, C.L., Coras, R., Lail, M., Blumcke, I., Livy, D.J., Malykhin, N., Gross, D.W., 2017. Development of a histologically validated segmentation protocol for the hippocampal body. NeuroImage 157, 219–232. https://doi.org/10.1016/j.neuroimage.2017.06.008

Stockmeier, C.A., Mahajan, G.J., Konick, L.C., Overholser, J.C., Jurjus, G.J., Meltzer, H.Y., Uylings, H.B.M., Friedman, L., Rajkowska, G., 2004. Cellular Changes in the Postmortem Hippocampus in Major Depression. Biol. Psychiatry 56, 640–650. https://doi.org/10.1016/j.biopsych.2004.08.022

Tardif, C.L., Devenyi, G.A., Amaral, R.S.C., Pelleieux, S., Poirier, J., Rosa-Neto, P., Breitner, J., Chakravarty, M.M., 2017. Regionally specific changes in the hippocampal circuitry accompany progression of cerebrospinal fluid biomarkers in preclinical Alzheimer's disease. Hum. Brain Mapp. 39, 971–984. https://doi.org/10.1002/hbm.23897

ten Donkelaar, H.J., Tzourio-Mazoyer, N., Mai, J.K., 2018. Toward a Common Terminology for the Gyri and Sulci of the Human Cerebral Cortex. Front. Neuroanat. 12, 93. https://doi.org/10.3389/fnana.2018.00093

Todtenkopf, M.S., Benes, F.M., 1998. Distribution of glutamate decarboxylase65 immunoreactive puncta on pyramidal and nonpyramidal neurons in hippocampus of schizophrenic brain. Synapse 29, 323–332. https://doi.org/10.1002/(SICI)1098-2396(199808)29:4<323::AID-SYN4>3.0.CO;2-7

Warren, D.E., Duff, M.C., Jensen, U., Tranel, D., Cohen, N.J., 2012. Hiding in plain view: lesions of the medial temporal lobe impair online representation. Hippocampus 22, 1577–1588. https://doi.org/10.1002/hipo.21000

Wisse, L.E.M., Daugherty, A.M., Olsen, R.K., Berron, D., Carr, V.A., Stark, C.E.L., Amaral, R.S.C., Amunts, K., Augustinack, J.C., Bender, A.R., Bernstein, J.D., Boccardi, M., Bocchetta, M., Burggren, A., Chakravarty, M.M., Chupin, M., Ekstrom, A., de Flores, R., Insausti, R., Kanel, P., Kedo, O., Kennedy, K.M., Kerchner, G.A., LaRocque, K.F., Liu, X., Maass, A., Malykhin, N., Mueller, S.G., Ofen, N., Palombo, D.J., Parekh, M.B., Pluta, J.B., Pruessner, J.C., Raz, N., Rodrigue, K.M., Schoemaker, D., Shafer, A.T., Steve, T.A., Suthana, N., Wang, L., Winterburn, J.L., Yassa, M.A., Yushkevich, P.A., la Joie, R., 2017. A harmonized segmentation protocol for hippocampal and parahippocampal subregions: why do we need one and what are the key goals? Hippocampus 27, 3–11. https://doi.org/10.1002/hipo.22671

Yushkevich, P.A., Amaral, R.S.C., Augustinack, J.C., Bender, A.R., Bernstein, J.D., Boccardi, M., Bocchetta, M., Burggren, A.C., Carr, V.A., Chakravarty, M.M., Chetelat, G., Daugherty, A.M., Davachi, L., Ding, S.-L., Ekstrom, A., Geerlings, M.I., Hassan, A., Huang, Y., Iglesias, E., La Joie, R., Kerchner, G.A., LaRocque, K.F.,

Libby, L.A., Malykhin, N., Mueller, S.G., Olsen, R.K., Palombo, D.J., Parekh, M.B., Pluta, J.B., Preston, A.R., Pruessner, J.C., Ranganath, C., Raz, N., Schlichting, M.L., Schoemaker, D., Singh, S., Stark, C.E.L., Suthana, N., Tompary, A., Turowski, M.M., Van Leemput, K., Wagner, A.D., Wang, L., Winterburn, J.L., Wisse, L.E.M., Yassa, M.A., Zeineh, M.M., 2015. Quantitative Comparison of 21 Protocols for Labeling Hippocampal Subfields and Parahippocampal Subregions in In Vivo MRI: Towards a Harmonized Segmentation Protocol. NeuroImage 111, 526–541. https://doi.org/10.1016/j.neuroimage.2015.01.004

Yushkevich, P.A., Avants, B.B., Pluta, J., Das, S., Minkoff, D., Mechanic-Hamilton, D., Glynn, S., Pickup, S., Liu, W., Gee, J.C., Grossman, M., Detre, J.A., 2009. A High-Resolution Computational Atlas of the Human Hippocampus from Postmortem Magnetic Resonance Imaging at 9.4 Tesla. NeuroImage 44, 385–398. https://doi.org/10.1016/j.neuroimage.2008.08.04

Zaidel, D., Esiri, Margaret, Harrison, Paul, 1997. Size, shape, and orientation of neurons in the left and right hippocampus: investigation of normal asymmetries and alterations in schizophrenia. Am. J. Psychiatry 154, 812–818. https://doi.org/10.1176/ajp.154.6.812

Zeidman, P., Lutti, A., Maguire, E.A., 2015. Investigating the functions of subregions within anterior hippocampus. Cortex J. Devoted Study Nerv. Syst. Behav. 73, 240–256. https://doi.org/10.1016/j.cortex.2015.09.002

Zeidman, P., Maguire, E.A., 2016. Anterior hippocampus: the anatomy of perception, imagination and episodic memory. Nat. Rev. Neurosci. 17, 173–182. https://doi.org/10.1038/nrn.2015.24

Zhou, Y., Shu, N., Liu, Y., Song, M., Hao, Y., Liu, H., Yu, C., Liu, Z., Jiang, T., 2008. Altered resting-state functional connectivity and anatomical connectivity of hippocampus in schizophrenia. Schizophr. Res. 100, 120–132. https://doi.org/10.1016/j.schres.2007.11.039

Zilles, K., Palomero-Gallagher, N., Amunts, K., 2015. Cytoarchitecture and Maps of the Human Cerebral Cortex. Brain Mapp. Encycl. Ref. 3, 115–135. https://doi.org/10.1016/B978-0-12-397025-1.00207-4

Zilles, K., Schleicher, A., Palomero-Gallagher, N., Amunts, K., 2002. 21 - Quantitative Analysis of Cyto- and Receptor Architecture of the Human Brain, in: Toga, A.W., Mazziotta, J.C. (Eds.), Brain Mapping: The Methods (Second Edition). Academic Press, San Diego, pp. 573–602. https://doi.org/10.1016/B978-012693019-1/50023-X

Figures

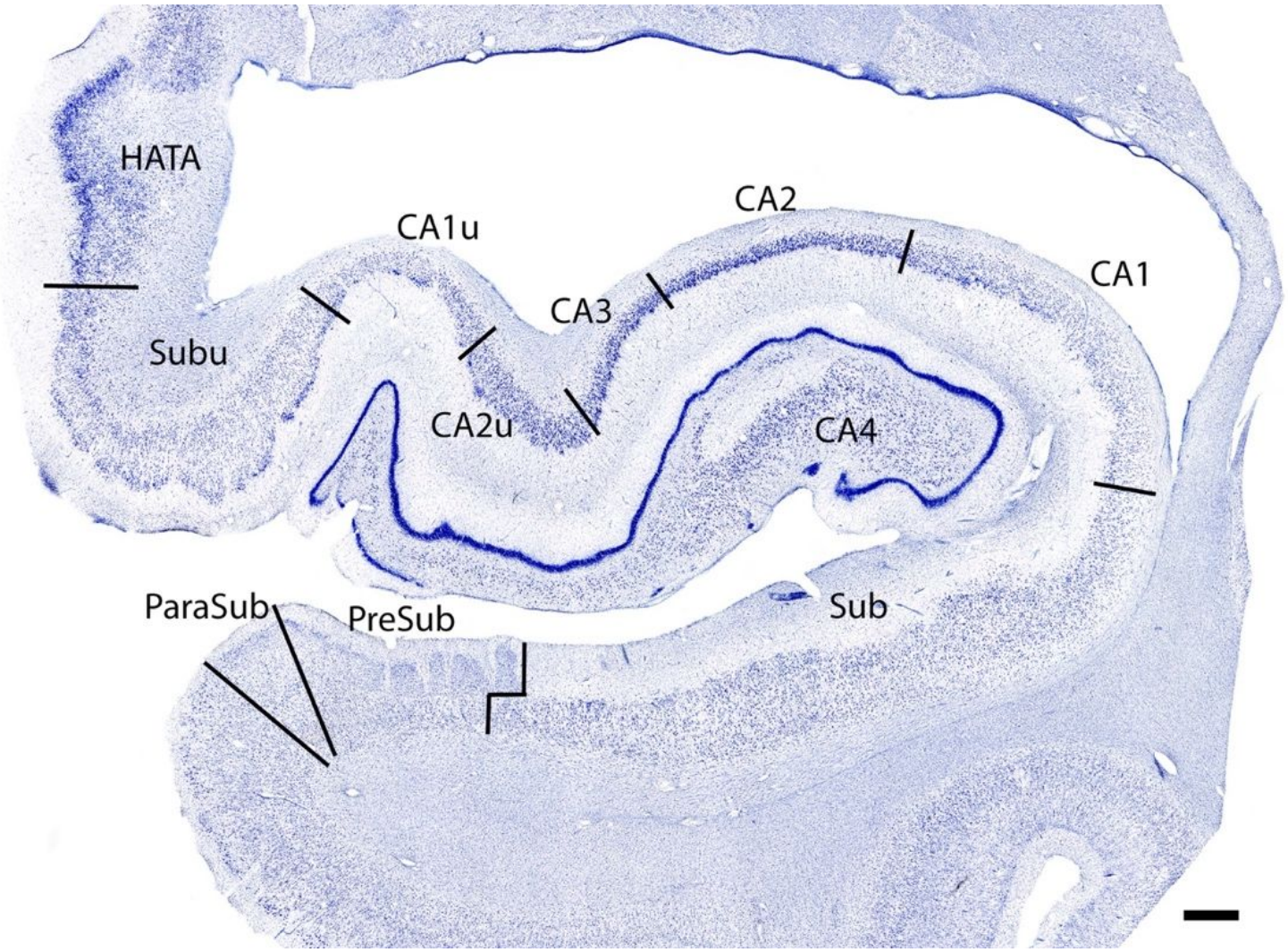

Figure 1

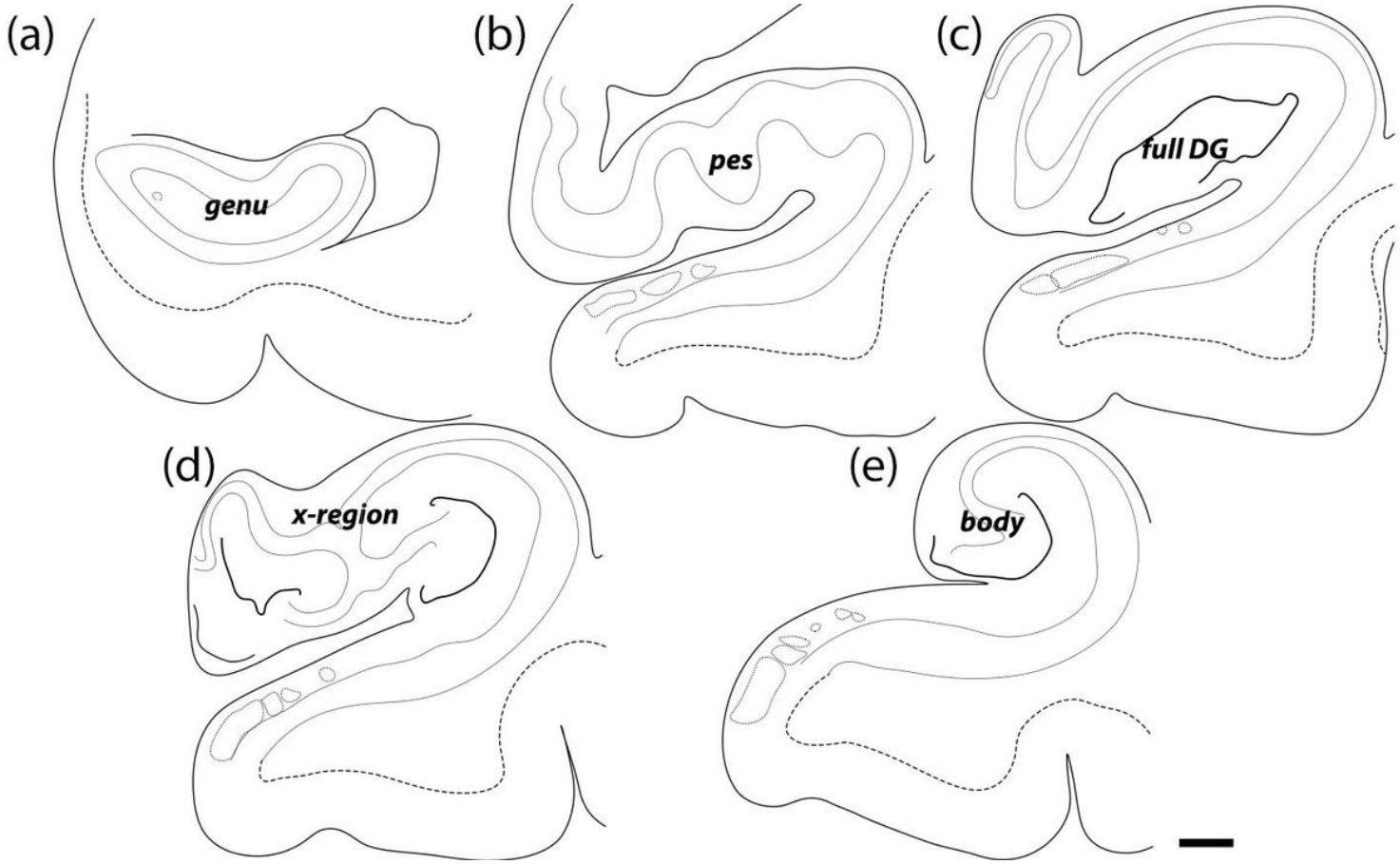

Figure 2

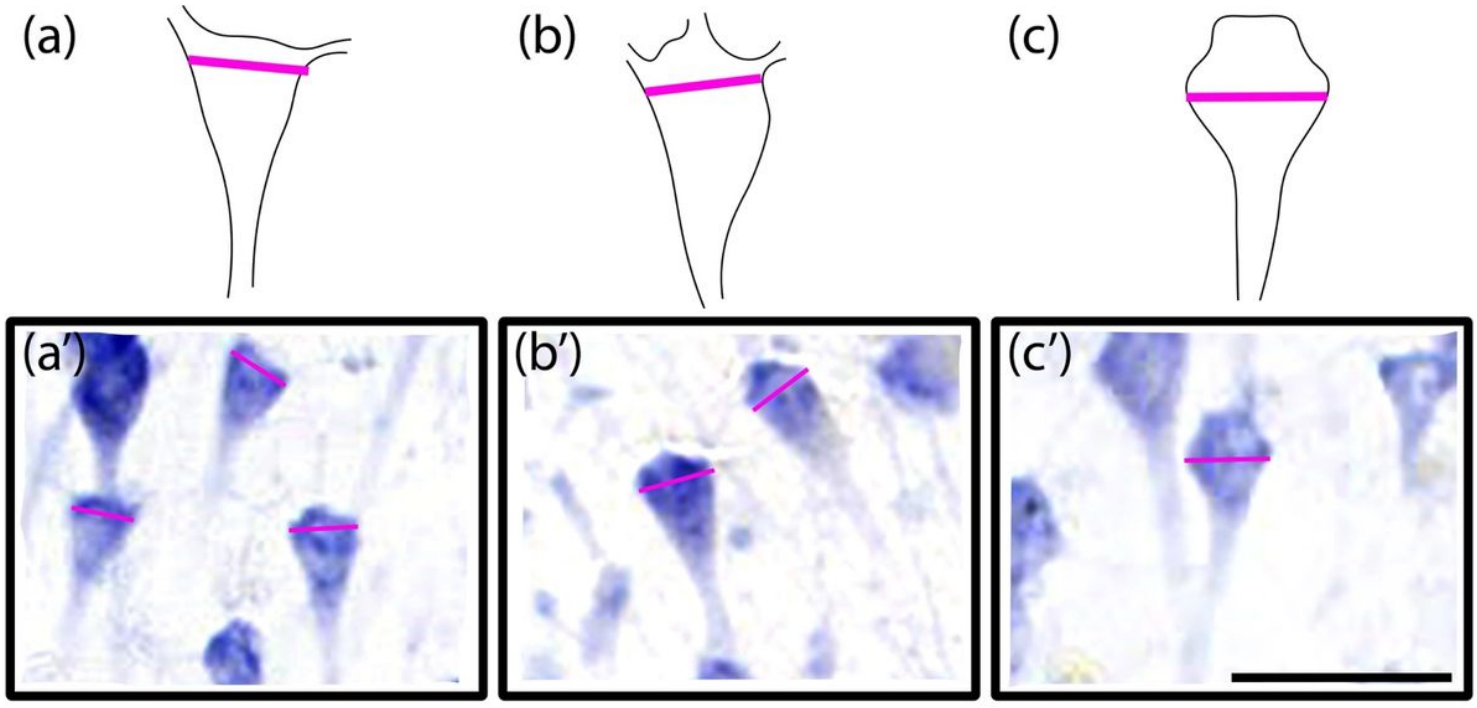

Figure 3

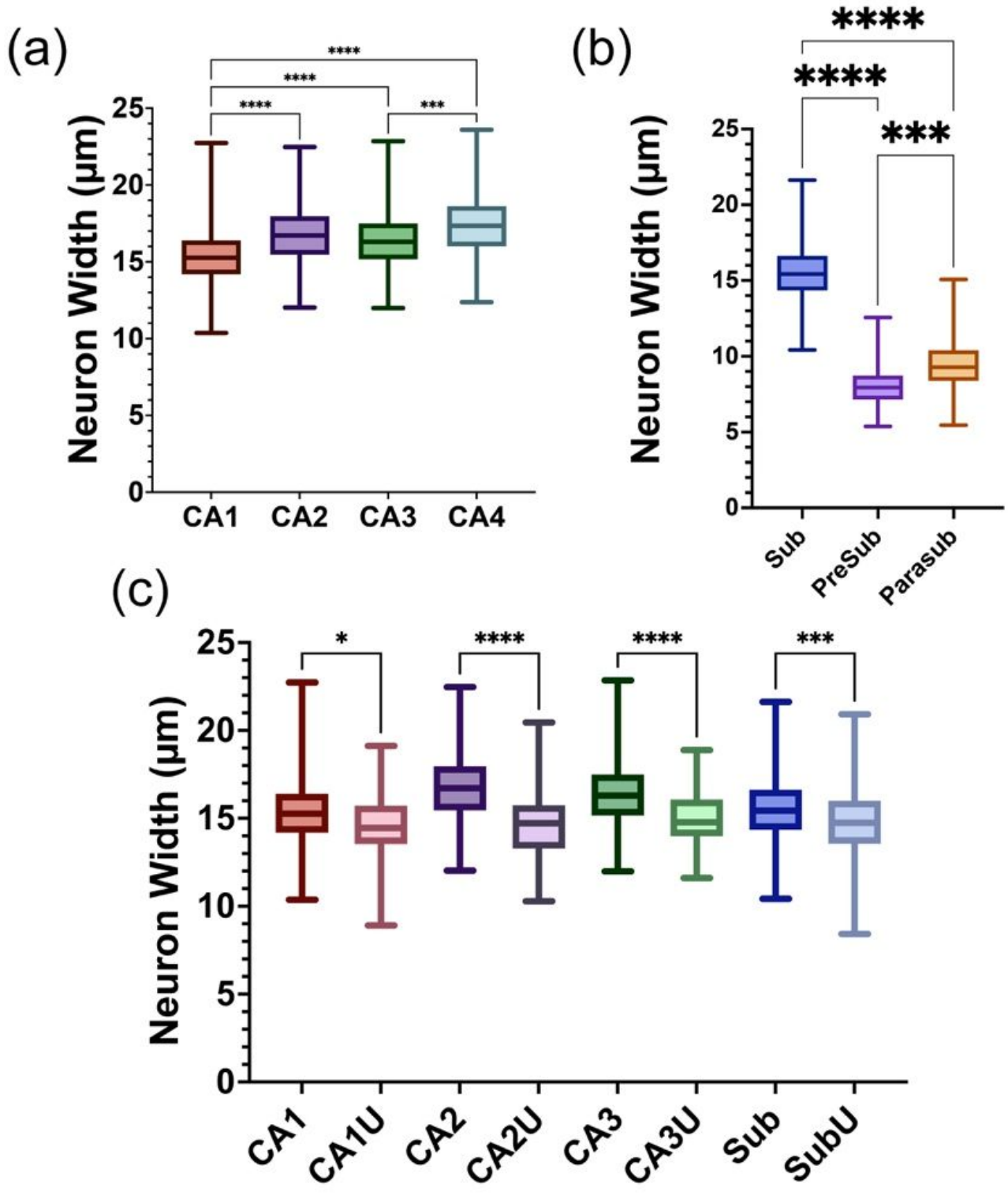
(a)
Neuron Width (µm)
0
5
10
15
20
25
****
****
****
***
CA1
CA2
CA3
CA4
(b)
Neuron Width (µm)
0
5
10
15
20
25
****
****
***
Sub
PreSub
Parasub
(c)
Neuron Width (µm)
0
5
10
15
20
25
*
****
****
***
CA1
CA1U
CA2
CA2U
CA3
CA3U
Sub
SubU

Figure 4

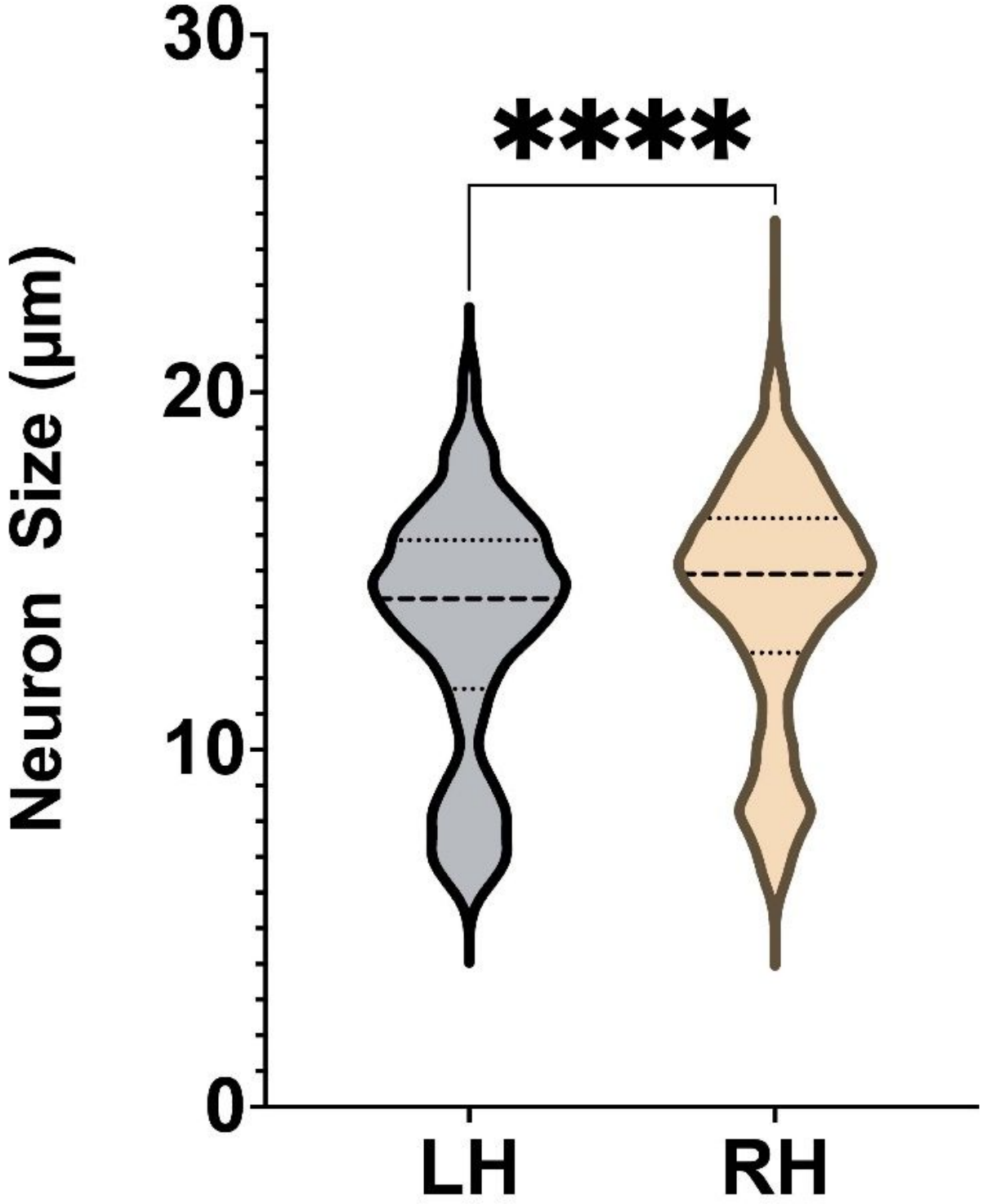

Figure 5

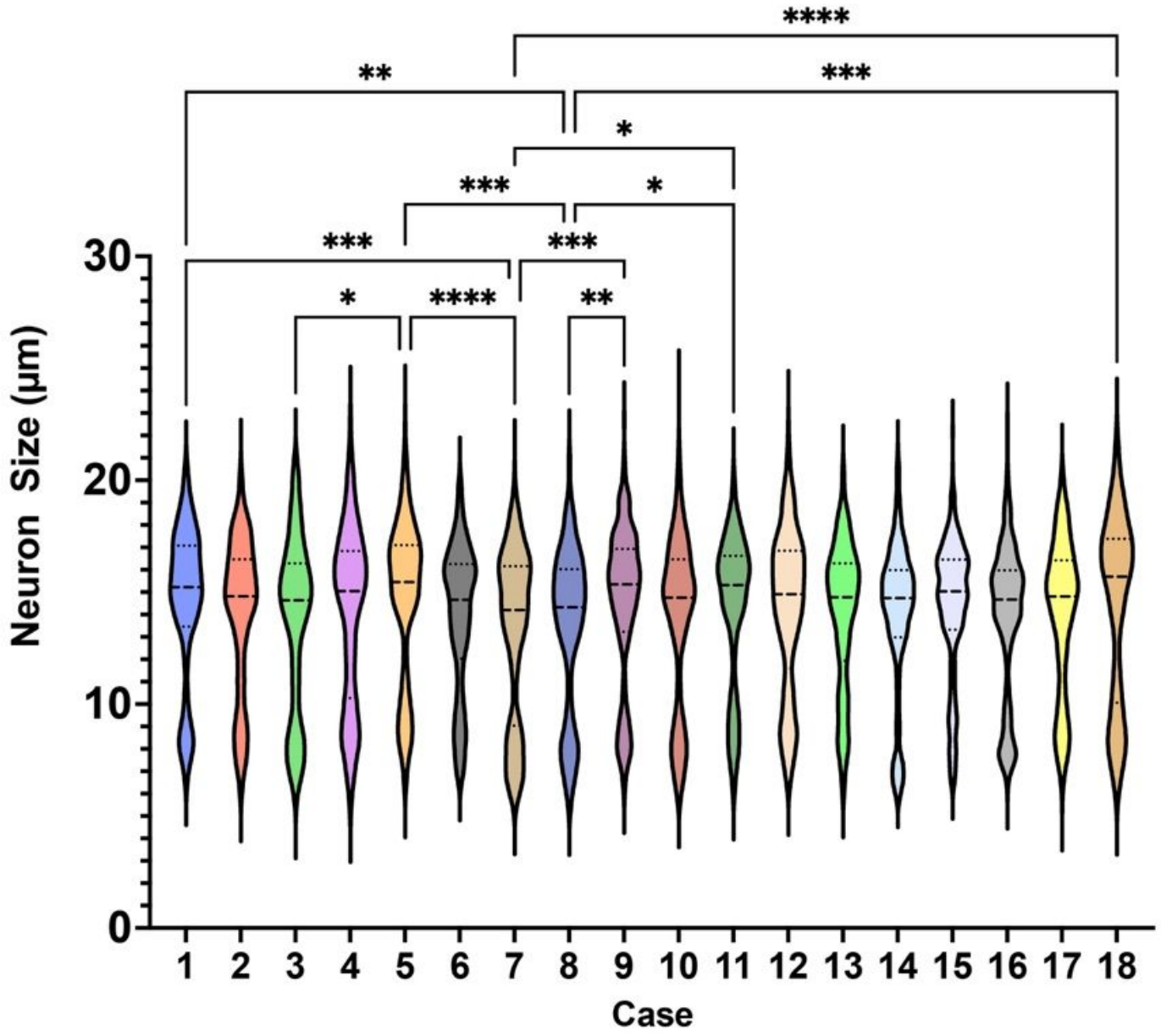
****
**
***
*
***
*
***
***
*
****
**
Neuron Size (μm)
30
20
10
0
1 2 3 4 5 6 7 8 9 10 11 12 13 14 15 16 17 18
Case

Figure 6